J Mol Model (2013) 19:1009–1018
DOI 10.1007/s00894-012-1616-8

ORIGINAL PAPER

Direct ab initio study on the rate constants of radical $C_2(A^3\Pi_u)+C_3H_8$ reaction

Rui-Ping Huo · Xiang Zhang · Xu-Ri Huang · Ji-Lai Li · Chia-Chung Sun

Received: 21 August 2012 / Accepted: 30 September 2012 / Published online: 30 October 2012

Abstract The mechanism and kinetics of the radical $^3C_2+C_3H_8$ reaction have been investigated theoretically by direct ab initio kinetics over a wide temperature range. The potential energy surfaces have been constructed at the CCSD(T)/B3//UMP2/B1 levels of theory. The electron transfer was also analyzed by quasi–restricted orbital (QRO) in detail. It was shown that all these channels proceed exclusively via hydrogen abstraction. The overall ICVT/SCT rate constants are in agreement with the available experimental results. The prediction shows that the secondary hydrogen of C_3H_8 abstraction by $^3C_2$ radical is the major pathway at low temperatures (below 700 K), while as the temperature increases, the primary hydrogen of C_3H_8 abstraction becomes more important and more favorable. A negative temperature dependence of the rate constants for the reaction of $^3C_2+C_3H_8$ was observed. The three–(k_3) and four–parameter (k_4) rate-temperature expressions were also provided within 243–2000 K to facilitate future experimental studies.

Keywords C_2 · Chemical kinetics · Rate constant · Variational transition–state theory

Electronic supplementary material The online version of this article (doi:10.1007/s00894-012-1616-8) contains supplementary material, which is available to authorized users.

R.-P. Huo · X.-R. Huang · J.-L. Li (✉) · C.-C. Sun
State Key Laboratory of Theoretical and Computational Chemistry, Institute of Theoretical Chemistry, Jilin University, Changchun 130023, People's Republic of China
e-mail: tcclab@gmail.com

X. Zhang
School of Chemistry and Materials Science, Shanxi Normal University, Linfen 041004, People's Republic of China

J.-L. Li
Department of Theoretical Chemistry, Lund University, Chemical Centre, P.O. Box 124, SE-221 00, Lund, Sweden

Introduction

The elementary reactions are often at the heart of important processes in combustion and catalysis. Despite their importance and intense studies in the past decades, many reactions are still poorly understood. Among these reactions, the gas phase kinetics of reactions of the dicarbon C_2 radical with a series of compounds have received increased attention recently not only because of its ubiquity in the universe, but its considerable importance in air pollution astrophysics, combustion, and atmospheric chemistry [1–12]. In addition, being one of the simplest diatomic molecules, the reactions of C_2 with small molecules could provide particularly useful knowledge for the detailed study of the elementary processes in the gaseous phase under wide temperature and pressure ranges, especially from a chemical kinetics point of view.

There are two low–lying electronic states for C_2 molecule, the singlet state $X^1\Sigma^+_g$ and the metastable triplet state $A^3\Pi_u$ (henceforth referred to as $^1C_2$ and $^3C_2$, respectively), which are separated by only 1.7 kcal mol^{-1} or 610 cm^{-1} [13]. Its electronic and structural properties and reactivity have been a subject of current interests and debates experimentally and theoretically [8–30]. However, there is still a long way to have complete understanding of its complexity. Understanding its chemistry and more specifically the temperature dependence of rate coefficients for reactions with other reagents is therefore of major interest hereto.

Up to now, a large number of experimental and theoretical investigations have been reported on the kinetics of $^3C_2$ and $^1C_2$ reactions with small hydrocarbons, such as CH_4, C_2H_2, C_2H_4, C_2H_6, C_3H_8, n–C_4H_{10}, i–C_4H_{10} and n–C_6H_{14} and so on [8–12, 16–18, 21, 24–30]. Among these reactions,

the kinetics behavior and reactivity of reaction of $^3C_2$ ($A^3\Pi_u$) with CH_4 [31] C_2H_6 [32] and CH_3OH [33] have been studied using direct ab initio kinetics methods by us very recently. For the $^3C_2+C_2H_6$ reaction, variational effect is small and nonclassical reflection effect is important to the H–atom abstraction in high temperature region; and variational effect is negligible and tunneling effect cooperating with the nonclassical reflection effect makes the rate constant temperature independent in low–temperature range [32]. For the $^3C_2+CH_4$ reaction, variational effect is to some extent large in lower temperature range, and small curvature and tunneling effect play important roles to the H–atom abstraction only at lower temperatures [31]. For the $^3C_2+C_3H_8$ reaction, experimental data is still rather limited hereto. To the best of our knowledge, the relevant data available in a wide temperature regime remains incomplete and uncertain and there is no available theoretical study. Several issues are still open. First, the experimental rate constants of the reaction $^3C_2+C_3H_8$ are only available over the temperature range 298–673 K($k=(7.90\pm2.62)\times10^{-19}T^{2.44\pm0.04}\times\exp((811.46\pm21.24)/T)$ (cm^3 $molecule^{-1}s^{-1}$). Second, positive or negative temperature dependence effects of the rate constants over a certain temperature range for C_3H_8 is also found but the tendencies versus the whole temperature range remains unclear [27, 28]. Furthermore, pronounced negative temperature dependences of the rate constants for the reactions of $^3C_2$ with larger hydrocarbons *n*–C_4H_{10}, *i*–C_4H_{10}, and *n*–C_6H_{14} have been detected below 323 K. However, the temperature dependences are still unclear for C_3H_8 due to limited rate constants available.

This reaction represents paradigmatic, challenging test case for chemical kinetics models from small hydrocarbons (CH_4 and C_2H_6) to higher hydrocarbons (C_4H_{10} and C_6H_{14}, etc.). These issues above stimulated our impetus, and we therefore performed direct ab initio kinetics study on the title reaction $^3C_2+C_3H_8$. Our aims are to explore the mechanisms, to obtain "accurate" theoretical rate constants and to see to what extent the theory can be compared with the available experimental results [16, 27, 28] over the wide temperature region 243–2000 K. In addition, the investigation of direct kinetics of C_2 radical reactions with other hydrocarbons is carried out in our laboratory. It is also expected to provide the temperature dependence of the rate constants over a wide temperature region for further experimental investigations.

Computational methods

The geometric parameters of the species involved in the title reaction were fully optimized using the unrestricted Møller–Plesset second–order perturbation theory (UMP2–FULL) [34] with the 6–311+G(2d,2p) basis set. All of the stationary points were identified for local minima and transition states by vibrational frequency analysis. Intrinsic reaction coordinate analyses [35] were performed to confirm the connection between transition states and designated reactants and products and to construct the minimum energy pathways with a gradient step–size of 0.05 $(amu)^{1/2}$ bohr. Then, the first and second energy derivatives were obtained to calculate the curvature of the reaction path and the generalized vibrational frequencies along the reaction pathways. On the basis of the optimized geometries, higher–level single–point energy calculations of the stationary points were performed by coupled–cluster theory [36] of triple excitations CCSD (T) level [37] with 6–311+G(2d,2p) (B1), 6–311++G (3df,2pd) (B2), and aug–cc–pVTZ (B3) basis sets, respectively. The T1 diagnostic values [38, 39] were calculated at the UCCSD(T)/aug-cc-pVTZ level to assess the reliability of the results of the single-reference wave function. As shown in Tables S1 and S2, the T1 diagnostic values are smaller than 0.045 [39] except for C_2H. This implies that all the structures have a single-reference character except for C_2H. Fortunately, the energy of C_2H is of less importance to this study. The CCSD(T) results are therefore reliable. All the electronic structure calculations were performed by Gaussian03 program package [40].

The theoretical rate constants were calculated with the POLYRATE 9.7 program package [41]. The theoretical rate constants were predicted by the conventional variational transition state theory (VTST) [42], improved canonical variational transition–state theory (ICVT) [43, 44], and improved canonical variational transition–state incorporating a small–curvature tunneling correction (ICVT/SCT) method [42]. The Euler single–step integrator with a step size of 0.005 $(amu)^{1/2}$ bohr is used to follow the MEP. A total of 24 points near the transition state (12 on reactants side and 12 on product side) were selected to obtain the potential surface information along the MEP. The curvature components were calculated using a quadratic fit to obtain the derivative of the gradient with respect to the reaction coordinate. Within the temperature range 243–2000 K, the rate constants at selected temperature points were calculated using mass–scaled Cartesian coordinate.

Quasi–restricted molecular orbital [45] of stationary points along the MEP were calculated by ORCA 2.8 program package [46] and plotted using Chimera [47].

Results and discussion

Stationary points

Hydrogen abstraction from C_3H_8 by $^3C_2$ can occur at three distinct sites [48], the in-plane primary H-atom and the out-of-plane primary H-atom abstractions leading to the n-

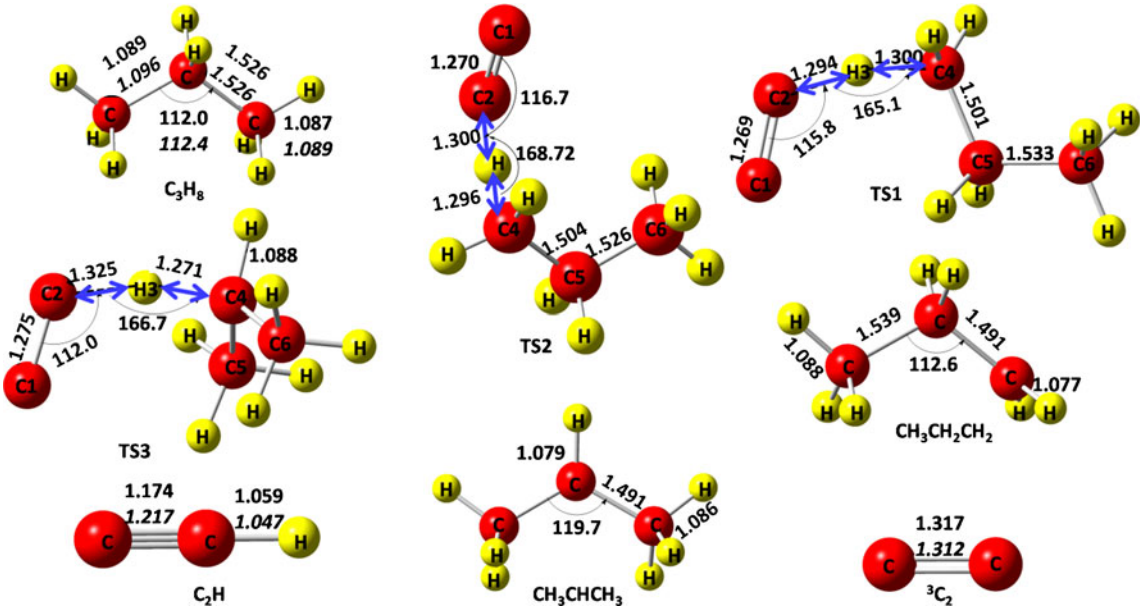

Fig. 1 Geometric parameters of various species involved in the title reaction. Bond length in angstrom and angle in degree. The normal and italics are at the UMP2/6–311+G(2d,2p) level, and experimental data, respectively. The *blue arrows* show the harmonic vibrational mode in the transition state. Experimental data: C_2, ref. [49]; C_3H_8, ref.[50]; C_2H, ref.[51]

propyl radical and either C_2H (1a and 2a) and with the secondary H-atom abstraction leading to isopropyl and C_2H (3a).

Channel 1 : In – plane primary hydrogen abstraction of C_3H_8

$$\mathbf{CH_3CH_2CH_3}+{}^3\mathbf{C_2} \rightarrow \mathbf{CH_3CH_2CH_2} + \bullet\mathbf{C_2H}\ (\text{in}-\text{plane primary}) \quad (1a)$$

Channel 2 : Out – of – plane primary hydrogen abstraction of C_3H_8

$$\mathbf{CH_3CH_2CH_3}+{}^3\mathbf{C_2} \rightarrow \mathbf{CH_3CH_2CH_2} + \bullet\mathbf{C_2H}\ (\text{out}-\text{of}-\text{plane primary}) \quad (2a)$$

Channel 3 : Secondary hydrogen abstraction of C_3H_8

$$\mathbf{CH_3CH_2CH_3}+{}^3\mathbf{C_2} \rightarrow \mathbf{CH_3CHCH_3} + \bullet\mathbf{C_2H}(\text{secondary}) \quad (3a)$$

The geometric parameters of the reactants, products and transition states of the title reaction were shown in Fig. 1. Selected bond lengths and angles and available experimental data were also given. The coordinates of the reactants, products and transition states are listed in Table S1 in Supporting information. The harmonic frequencies of all the species involved in the title reaction and available experimental values were also listed in Supporting information (Table S2). The geometry parameters of all species calculated by UMP2 method are reasonably consistent with available experimental data. As shown in Fig. 1, we can find that in the transition structure TS1 in channel 1, the length of bond C4–H3 to be broken increases by 19.5 % compared with the equilibrium bond length of C–H in C_3H_8. The C2–H3 bond to be formed is 1.22 times the equilibrium bond length of C–H in the product $\bullet C_2H$. Hence, the smaller stretch of the breaking bond than that of the forming bond

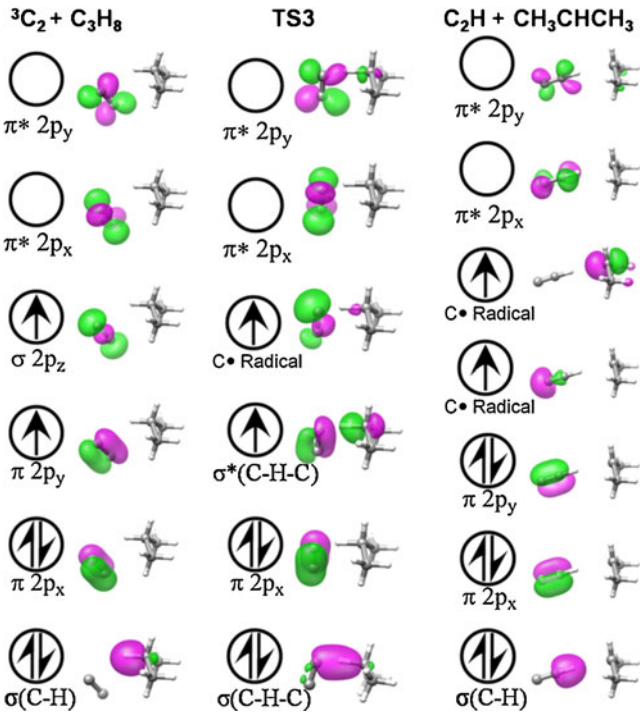

Fig. 2 Schematic MO diagrams of reactants ($^3C_2$+C_3H_8), transition state (TS3) and products ($\bullet C_2H$+$\bullet CH_3CHCH_3$)

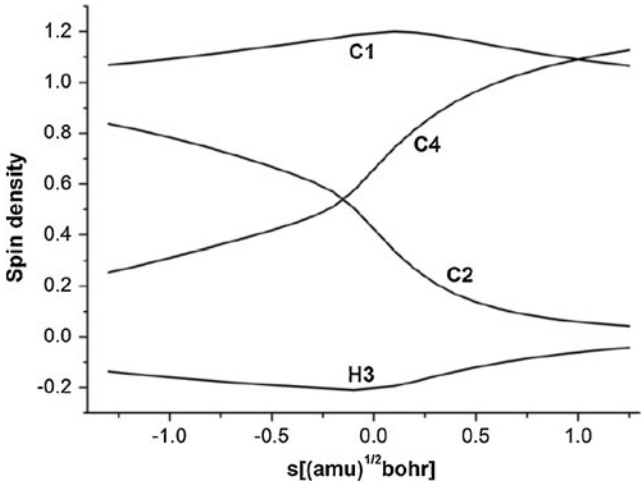

Fig. 3 The change of atomic spin densities on C1, C2, H3 and C4 in **channel 3** obtained from selected points on IRC pathways

indicates a reactant–like transition state, i.e., the H–abstraction channel process overcomes an early transition state. Notably, the three atoms involved in the transition state TS1 is almost collinear (∠C2H3C4=165.1°) and the dihedral angel ∠C1-C2-C4-C5 is 14.8°. TS1 possesses one and only one imaginary frequency 1220i cm^{-1}, indicating that the transition state is a real first–order saddle point. On the other hand, we can find that TS2 in channel 2 features quite similar characters and the description is omitted here.

For the transition state TS3 in channel 3, the C4–H3 bond of C_3H_8 is stretched by 17 % over its equilibrium structure in C_3H_8 and the C2–H3 bond to be formed is about 1.3 times the equilibrium bond length of C–H in the product $•C_2H$. Thus, the smaller stretch of the breaking bond than that of the forming bond also indicates a reactant–like transition state. That is to say, the secondary H–atom abstraction channel process is also via an early transition state. The three atoms involved in TS3 is almost collinear and the angle ∠C2H3C4 is 166.7°. TS3 possesses one and only one imaginary frequency 881i cm^{-1}, indicating that the transition state is a real first–order saddle point. Furthermore, the harmonic vibrational frequencies of all the reactants, and products at the MP2/6–311+G(2d,2p) level are also in good agreement with available experimental results [49–51].

Electron transfer behaviors

Analysis of the changes of the electronic structure along the reaction coordinates could provide further details about the reaction mechanism and gain deeper insights into the origin of the relatively low energy barrier. The detailed electron transfer analysis was therefore carried out along the minimal energy pathway by quasi–restricted molecular orbital calculations by ORCA program. Figure S1 and Fig. 2 show the schematic frontier molecular orbital (FMO) diagrams for the reactants, transition states and products involved in channel 1, channel 2, and channel 3, respectively. As shown in Fig. 2, the triplet C_2 moiety has one half-occupied orbital on each C atom at the starting point. As the $^3C_2$ and C_3H_8 gradually approach each other, the σ_{C-H} bond of C_3H_8 is going to attack the half–occupied π–$2p_y$ orbital in $^3C_2$ moiety. During this process, one β–spin electron in the σ_{C-H} bond of C_3H_8 is shifted to C2 atom of $^3C_2$ gradually. The α–spin electron in π–$2p_y$ orbital together with the β–spin electron carried by hydrogen atom forms a new $\sigma_{(C-H-C)}$ bond and $\sigma^*_{(C-H-C)}$ in the C2–H3–C4 moiety which possesses a collinear structure in the transition state TS1, TS2 and/or TS3. Afterward, the C_3H_8 C–H is broken completely and a new C–H bond is formed in $•C_2H$ moiety which possesses a bent angle structure. Finally, the electron redistribution among the $•C_2H$ array leads to the energetically more stable linear structure with two π bonds. Schematically as shown in Fig. 2,

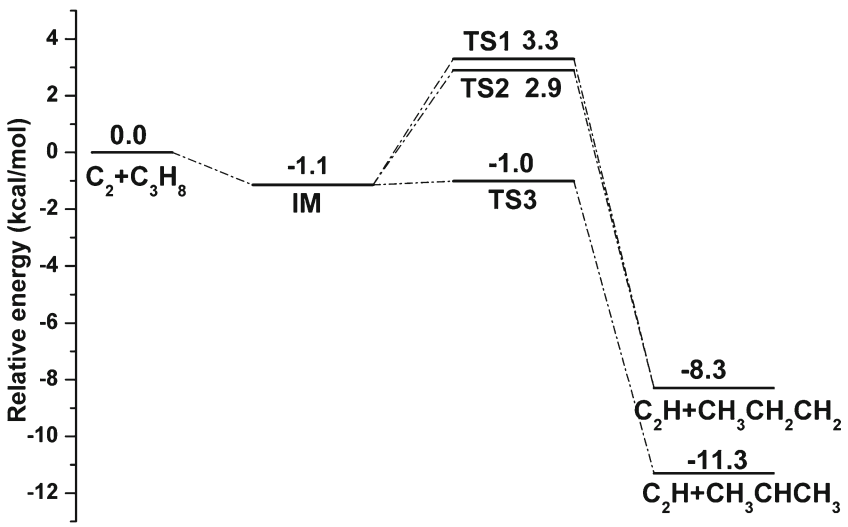

Fig. 4 Potential energy profiles for the title reaction with ZPE correction at CCSD(T)/B3//UMP2/B1 level

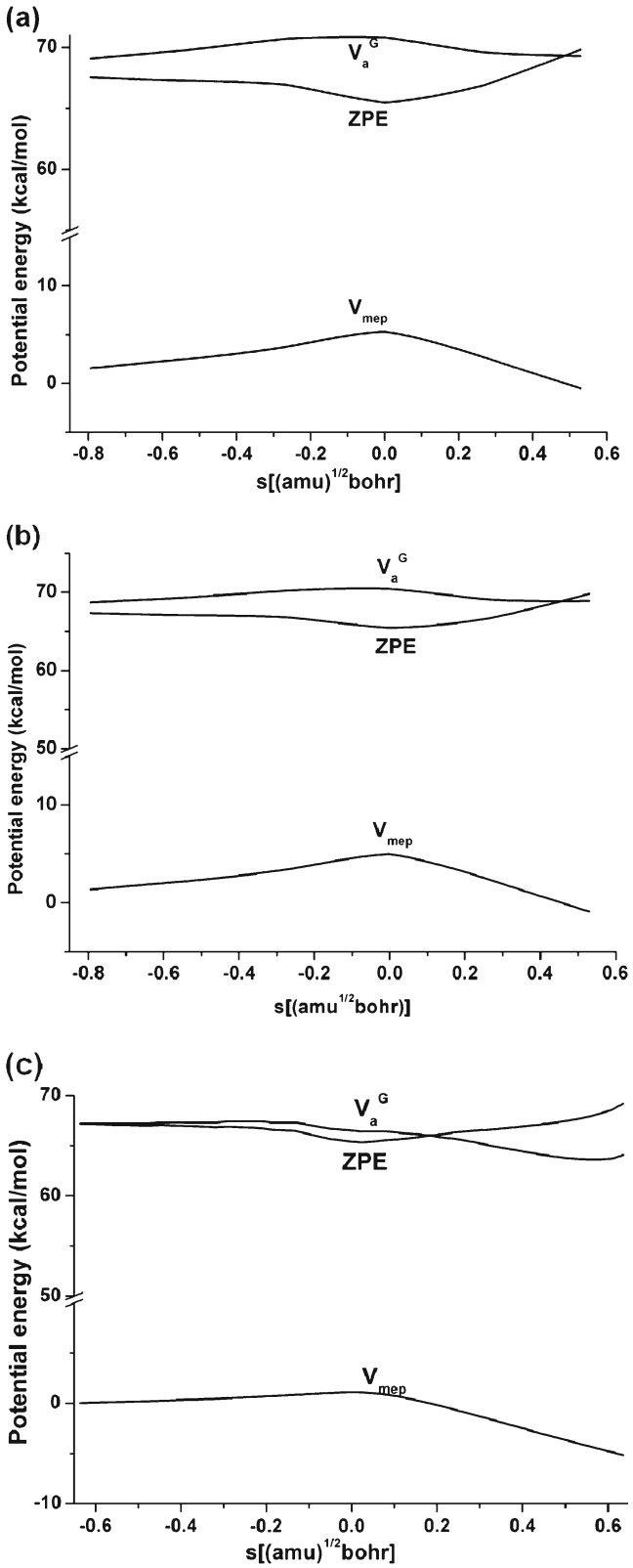

Fig. 5 Classical potential energy curve (V_{MEP}), ground–state vibrationally adiabatic curve (), and ZPE curve as functions of s [(amu)$^{1/2}$bohr] at the CCSD(T)/B3//UMP2/B1 levels for **channel 1** (**a**), **channel 2** (**b**), and **channel 3** (**c**) of the title reaction

one proton and β-electron in the C–H bond of C_3H_8 are transferred concomitantly to the singly occupied orbital on $^3C_2$ radical. By analysis of the corresponding molecular orbital, we can draw the conclusion that these three reaction pathways take place through the classical hydrogen–atom transfer (HAT) mechanism and electron transfer behaviors in channel 1, channel 2 and channel 3 are fundmentally similar.

The spin density changes upon the reaction channels are plotted in Fig. 3 and Fig. S2 (Supporting information). These spin density curves are very similar in shape. As the reaction goes on, the spin density of C4 increases concomitantly whereas it decreases on C2. Moreover, the spin densities of C1 and H3 are nearly unchanged. To sum up, the overall mechanism of the title reaction can be better described as the following: as C_3H_8 and $^3C_2$ gradually approach each other, the primary and secondary hydrogen-atom in C_3H_8 are abstracted by $^3C_2$, leading to $CH_3CH_2CH_2$ and/or CH_3CHCH_3 and the radical $\bullet C_2H$ generation.

Energetics

The barriers and reaction energies of the three channels obtained at the CCSD(T)/B3//UMP2/B1 levels in the present study were plotted in Fig. 4. The total energy of the reactants $^3C_2+C_3H_8$ was set to zero as a reference for other species involved in the title reaction. As shown in Fig. 4, the calculated barrier heights with zero–point energy (ZPE) at the CCSD(T)/B3//UMP2/B1 level are to be 3.3, 2.9 and −1.0 kcal mol^{-1} for channel 1, channel 2 and channel 3, respectively. Channel 3 is typically barrierless. Due to the lowest barrier height of channel 3 and the 4.3 and 3.9 kcal mol^{-1} high rate–controlling energy barrier TS1 and TS2 in channels 1 and 2, respectively, it is obvious that channel 3 should be considered as a dominant pathway under standard conditions.

In order to construct reliable MEPs for subsequent rate constant calculations, we further refined the single point energies of stationary points using CCSD(T) method with basis sets B1, B2 and B3, respectively. The electronic structural energies, zero–point correction energies and relative energies of all stationary points at various levels of theory are given in the Supporting information (Tables S3–S5). As shown in Table S5, among the three levels of theory, the energy barrier heights ΔE of TS3 decreases (−0.3→−1.8→−2.1 kcal mol^{-1}) along with the increasing of basis sets B1→B2→B3, and the CCSD(T)/B3 gives the lowest effective energy barrier −2.1 kcal mol^{-1}. Notably, this lies in the fact that the maximum energy point on MEP at higher level, e.g., CCSD(T), is generally not the same as that of the transition state obtained at the lower level. IRCMax correction is therefore required when the transition state displacement is substantial [29,

Table 1 Calculated rate constants for the $C_2+C_3H_8 \rightarrow C_2H+CH_3CH_2CH_2$ (**channel 1** and **2**) and $C_2+C_3H_8 \rightarrow C_2H+CH_3CHCH_3$ (**channel 3**) reaction in the temperature range 243–2000 K (cm^3 $molecule^{-1}s^{-1}$) at the UCCSD(T)/aug-cc-pVTZ//UMP2/6–311+G(2d,2p) level

Species	Channel 1 (k_1)			Channel 2 (k_2)			Channel 3 (k_3)		
T(K)	TST	ICVT	ICVT/SCT	TST	ICVT	ICVT/SCT	ICVT	ICVT/SCT	ICVT/SCT
243	8.65×10^{-14}	8.67×10^{-14}	1.45×10^{-13}	1.51×10^{-13}	6.51×10^{-14}	1.05×10^{-13}	2.06×10^{-10}	2.88×10^{-10}	2.88×10^{-10}
245	9.60×10^{-14}	9.39×10^{-14}	1.50×10^{-13}	1.56×10^{-13}	6.72×10^{-14}	1.07×10^{-13}	2.01×10^{-10}	2.81×10^{-10}	2.81×10^{-10}
248	1.02×10^{-14}	9.92×10^{-14}	1.57×10^{-13}	1.64×10^{-13}	7.04×10^{-14}	1.11×10^{-13}	1.93×10^{-10}	2.72×10^{-10}	2.72×10^{-10}
253	1.13×10^{-13}	1.06×10^{-13}	1.71×10^{-13}	1.78×10^{-13}	7.60×10^{-14}	1.18×10^{-13}	1.82×10^{-10}	2.56×10^{-11}	2.56×10^{-11}
263	1.36×10^{-13}	1.29×10^{-13}	2.00×10^{-13}	2.08×10^{-13}	8.81×10^{-14}	1.32×10^{-13}	1.63×10^{-10}	2.31×10^{-11}	2.31×10^{-11}
298	2.45×10^{-13}	2.34×10^{-13}	3.30×10^{-13}	3.37×10^{-13}	1.40×10^{-13}	1.93×10^{-13}	1.21×10^{-10}	1.72×10^{-11}	1.72×10^{-11}
299	2.49×10^{-13}	2.37×10^{-13}	3.34×10^{-13}	3.41×10^{-13}	1.42×10^{-13}	1.95×10^{-13}	1.20×10^{-10}	1.71×10^{-11}	1.71×10^{-11}
323	3.52×10^{-13}	3.38×10^{-13}	4.53×10^{-13}	4.56×10^{-13}	1.87×10^{-13}	2.46×10^{-13}	1.04×10^{-10}	1.48×10^{-11}	1.48×10^{-11}
370	6.37×10^{-13}	6.13×10^{-13}	7.68×10^{-13}	7.52×10^{-13}	3.03×10^{-13}	3.74×10^{-13}	8.61×10^{-11}	1.22×10^{-11}	1.22×10^{-11}
373	6.59×10^{-13}	6.35×10^{-13}	7.93×10^{-13}	7.74×10^{-13}	3.12×10^{-13}	3.84×10^{-13}	8.54×10^{-11}	1.20×10^{-11}	1.20×10^{-11}
386	7.62×10^{-13}	7.35×10^{-13}	9.04×10^{-13}	8.76×10^{-13}	3.52×10^{-13}	4.27×10^{-13}	8.26×10^{-11}	1.16×10^{-11}	1.16×10^{-11}
423	1.12×10^{-12}	1.08×10^{-12}	1.28×10^{-12}	1.22×10^{-12}	4.84×10^{-13}	5.69×10^{-13}	7.72×10^{-11}	1.08×10^{-11}	1.08×10^{-11}
435	1.25×10^{-12}	1.21×10^{-12}	1.43×10^{-12}	1.34×10^{-12}	5.34×10^{-13}	6.22×10^{-13}	7.62×10^{-11}	1.06×10^{-11}	1.06×10^{-11}
441	1.32×10^{-12}	1.28×10^{-12}	1.50×10^{-12}	1.41×10^{-12}	5.60×10^{-13}	6.49×10^{-13}	7.57×10^{-11}	1.06×10^{-11}	1.06×10^{-11}
473	1.76×10^{-12}	1.71×10^{-12}	1.96×10^{-12}	1.81×10^{-12}	7.13×10^{-13}	8.12×10^{-13}	7.43×10^{-11}	1.03×10^{-11}	1.03×10^{-11}
523	2.63×10^{-12}	2.56×10^{-12}	2.87×10^{-12}	2.58×10^{-12}	1.01×10^{-12}	1.12×10^{-12}	7.45×10^{-11}	1.04×10^{-11}	1.04×10^{-11}
573	3.77×10^{-12}	3.67×10^{-12}	4.04×10^{-12}	3.55×10^{-12}	1.38×10^{-12}	1.51×10^{-12}	7.68×10^{-11}	1.07×10^{-11}	1.07×10^{-11}
623	5.22×10^{-12}	5.09×10^{-12}	5.52×10^{-12}	4.75×10^{-12}	1.85×10^{-12}	1.99×10^{-12}	8.07×10^{-11}	1.12×10^{-11}	1.12×10^{-11}
673	7.02×10^{-12}	6.86×10^{-12}	7.35×10^{-12}	6.22×10^{-12}	2.41×10^{-12}	2.57×10^{-12}	8.58×10^{-11}	1.18×10^{-11}	1.18×10^{-11}
700	8.16×10^{-12}	7.98×10^{-12}	8.51×10^{-12}	7.13×10^{-12}	2.76×10^{-12}	2.93×10^{-12}	8.91×10^{-11}	1.22×10^{-11}	1.22×10^{-11}
800	1.35×10^{-11}	1.32×10^{-11}	1.39×10^{-11}	1.13×10^{-11}	4.37×10^{-12}	4.57×10^{-12}	1.04×10^{-10}	1.41×10^{-11}	1.41×10^{-11}
1000	3.09×10^{-11}	3.03×10^{-11}	3.13×10^{-11}	2.44×10^{-11}	9.39×10^{-12}	9.67×10^{-12}	1.45×10^{-10}	1.95×10^{-11}	1.95×10^{-11}
1200	5.97×10^{-11}	5.87×10^{-11}	6.00×10^{-11}	4.54×10^{-11}	1.75×10^{-11}	1.78×10^{-11}	2.02×10^{-10}	2.69×10^{-11}	2.69×10^{-11}
1500	1.31×10^{-10}	1.29×10^{-10}	1.31×10^{-10}	9.57×10^{-11}	3.69×10^{-11}	3.74×10^{-11}	3.19×10^{-10}	4.20×10^{-11}	4.20×10^{-11}
2000	3.47×10^{-10}	3.41×10^{-10}	3.44×10^{-10}	2.44×10^{-10}	9.46×10^{-11}	9.53×10^{-11}	6.10×10^{-10}	7.93×10^{-11}	7.93×10^{-11}

52, 53]. In channel 3, the highest point (s= −0.1985) gives positive barrier (0.1 kcal mol^{-1}) consistently by IRCMax method at CCSD(T)/B3//MP2 level in current study. A trend apparent from these results is that the CCSD(T) results are sensitive to the selected basis set, larger basis sets yielding lower barrier height. According to our experience [28, 29, 54], the barrier height of CCSD(T)/B3 should be more reliable and this is also verified in the subsequent rate constants calculations. The calculated reaction enthalpies (H_{298}) of the $^3C_2+C_3H_8$ reactions are listed in the Supporting information (Table S5). The CCSD(T) methods estimate channel 3 exothermic by −10.3,–11.4 and −10.9 kcal mol^{-1} at the CCSD(T)/B1//UMP2, CCSD(T)/B2//UMP2 and CCSD (T)/B3//UMP2 levels, respectively. Considering the efficiency and precision, it is therefore safe to make the conclusion that the combination of the CCSD(T)/B3//UMP2/B1 methods could provide satisfactory results for this work. So, we refined the SPE of selected points on the UMP2/B1 MEPs at the CCSD(T)/B3 level for the following rate constant calculations.

Kinetics calculations

Figure 5 depicts the plot of the classical potential energy curve $V_{MEP(s)}$, the vibrationally adiabatic ground–state potential curve V_a^G $_{(s)}$, and the zero–point energy (ZPE) profile as functions of the intrinsic reaction coordinate $(amu)^{1/2}$ bohr at the CCSD(T)/B3//UMP2/B1 level, where $V_a^G = V_{MEP} + ZPE$. In Fig. 5a,b and c, we can see that the V_a^G $_{(s)}$ and V_{MEP} curves are very similar in shape, and all the locations of the maximum values of the three curves are at s=0.0, implying variational effects are negligible in the three channels. This is also in good agreement with the reaction of $^3C_2+C_2H_6$ [32]. The ZPE curve drops near s= 0.0 $(amu)^{1/2}$ bohr and shows a noticeable variation with s. This drop offers a good explanation of the lower effect barrier height and the more flat V_a^G curve, implying the

Table 2 The overall rate constants (k) along with the experimental data for the $C_2+C_3H_8$ reaction in the temperature range 243–2000 K (cm^3 $molecule^{-1}s^{-1}$) at the UCCSD(T)/aug–cc–pVTZ//UMP2/6–311w+G(2d,2p) level

T(K)	TST	ICVT	ICVT/SCT	Expt[16]	Expt[28]
243	2.06×10^{-10}	2.90×10^{-10}	2.91×10^{-10}		
245	2.01×10^{-10}	2.83×10^{-10}	2.84×10^{-10}		
248	1.93×10^{-10}	2.74×10^{-10}	2.75×10^{-10}		
253	1.82×10^{-10}	2.58×10^{-11}	2.59×10^{-11}		
263	1.63×10^{-10}	2.33×10^{-11}	2.34×10^{-11}		
298	1.22×10^{-10}	1.76×10^{-11}	1.77×10^{-11}	$1.35\pm0.04\times10^{-11}$	$1.35\pm0.02\times10^{-11}$
299	1.21×10^{-10}	1.75×10^{-11}	1.76×10^{-11}	$1.35\pm0.04\times10^{-11}$	
300	1.21×10^{-10}	1.75×10^{-11}	1.76×10^{-11}		
323	1.05×10^{-10}	1.53×10^{-11}	1.55×10^{-11}		$1.32\pm0.02\times10^{-11}$
370	8.75×10^{-11}	1.31×10^{-11}	1.33×10^{-11}	$1.41\pm0.04\times10^{-11}$	
373	8.68×10^{-11}	1.29×10^{-11}	1.32×10^{-11}		$1.35\pm0.03\times10^{-11}$
386	8.42×10^{-11}	1.27×10^{-11}	1.29×10^{-11}		
423	7.95×10^{-11}	1.24×10^{-11}	1.26×10^{-11}		$1.43\pm0.02\times10^{-11}$
441	7.84×10^{-11}	1.24×10^{-11}	1.27×10^{-11}	$1.50\pm0.04\times10^{-11}$	
473	7.89×10^{-11}	1.29×10^{-11}	1.32×10^{-11}		$1.51\pm0.02\times10^{-11}$
523	7.87×10^{-11}	1.36×10^{-11}	1.40×10^{-11}		$1.65\pm0.03\times10^{-11}$
573	8.09×10^{-11}	1.51×10^{-11}	1.56×10^{-11}		$1.80\pm0.02\times10^{-11}$
623	8.56×10^{-11}	1.72×10^{-11}	1.77×10^{-11}		$1.98\pm0.02\times10^{-11}$
673	9.25×10^{-11}	1.99×10^{-11}	2.05×10^{-11}		$2.16\pm0.03\times10^{-11}$
700	1.00×10^{-11}	2.22×10^{-11}	2.29×10^{-11}		
800	1.15×10^{-9}	2.82×10^{-11}	2.90×10^{-11}		
900	1.36×10^{-10}	3.91×10^{-11}	4.01×10^{-11}		
1000	2.00×10^{-10}	5.92×10^{-11}	6.05×10^{-11}		
1200	3.07×10^{-10}	1.03×10^{-10}	1.05×10^{-10}		
1500	5.46×10^{-10}	2.08×10^{-10}	2.10×10^{-10}		
2000	1.20×10^{-9}	5.15×10^{-10}	5.19×10^{-10}		

quantum effect would be large for the rate constants calculations. The variational and quantum effects on the rate constants will be tested in the following study (*infra*). This behavior is typical of hydrogen abstraction reaction, and the variation with s is mainly due to a fall in H••••$CH_2CH_2CH_3$ stretching corresponding to the normal mode breaking during the reaction, and evolving to the C_2••••H stretching mode forming in the product (reactive mode). On the other hand, in Fig. 5c, although the ZPE curve also drops near s= 0.0 $(amu)^{1/2}$ bohr, it shows a noticeable variation with s. The V_a^G (s) and V_{MEP} curves are different in shape because the V_{MEP} is too flat and the drop point of ZPE curve and the top point of the V_{MEP} overlaps with each other, indicating that the variational effect plays an important role for channel 3. This behavior is typical of hydrogen abstraction reaction, and the variation with s is mainly due to a fall in H••••CH $(CH_3)_2$ stretching corresponding to the normal mode breaking during the reaction, and evolving to the C_2••••H stretching mode forming in the product (reactive mode).

The rate constants for the three reaction channels were calculated by using the conventional transition–state theory (TST), improved canonical variational transition–state theory (ICVT), and ICVT with the small–curvature tunneling correction (SCT) over the temperature range 243–2000 K at the CCSD(T)/B3//UMP2/B1 levels of theory. The calculated ICVT/SCT overall rate constants are also provided by summing up the individual rate constants associated with the three channels. These data are listed in Tables 1 and 2, and the available experimental rate constants are also given [8, 16, 28]. The predicted rate constants in the temperature range 243–2000 K and experimental values are plotted as functions of the reciprocal of temperature as shown in Fig. 6. In Fig. 6a and b, the rate constants of TST and ICVT are nearly the same over the whole temperature range, which means that the variational effect for channel 1 and channel 2 are very small and almost negligible. The ICVT/SCT rate constants are obviously greater than that of the ICVT values in the range of 243–573 K. For example, the $k_{ICVT/SCT}/k_{ICVT}$ ratios for channel 1 are 1.67, 1.41 and 1.10 and for channel 2 are 1.62, 1.38 and 1.09 at 243, 298 and 573 K, respectively. Therefore, SCT correction plays an important role and should be considered in rate constant calculations in low–temperature range. In Fig. 6c, there is a distinct difference throughout the entire temperature

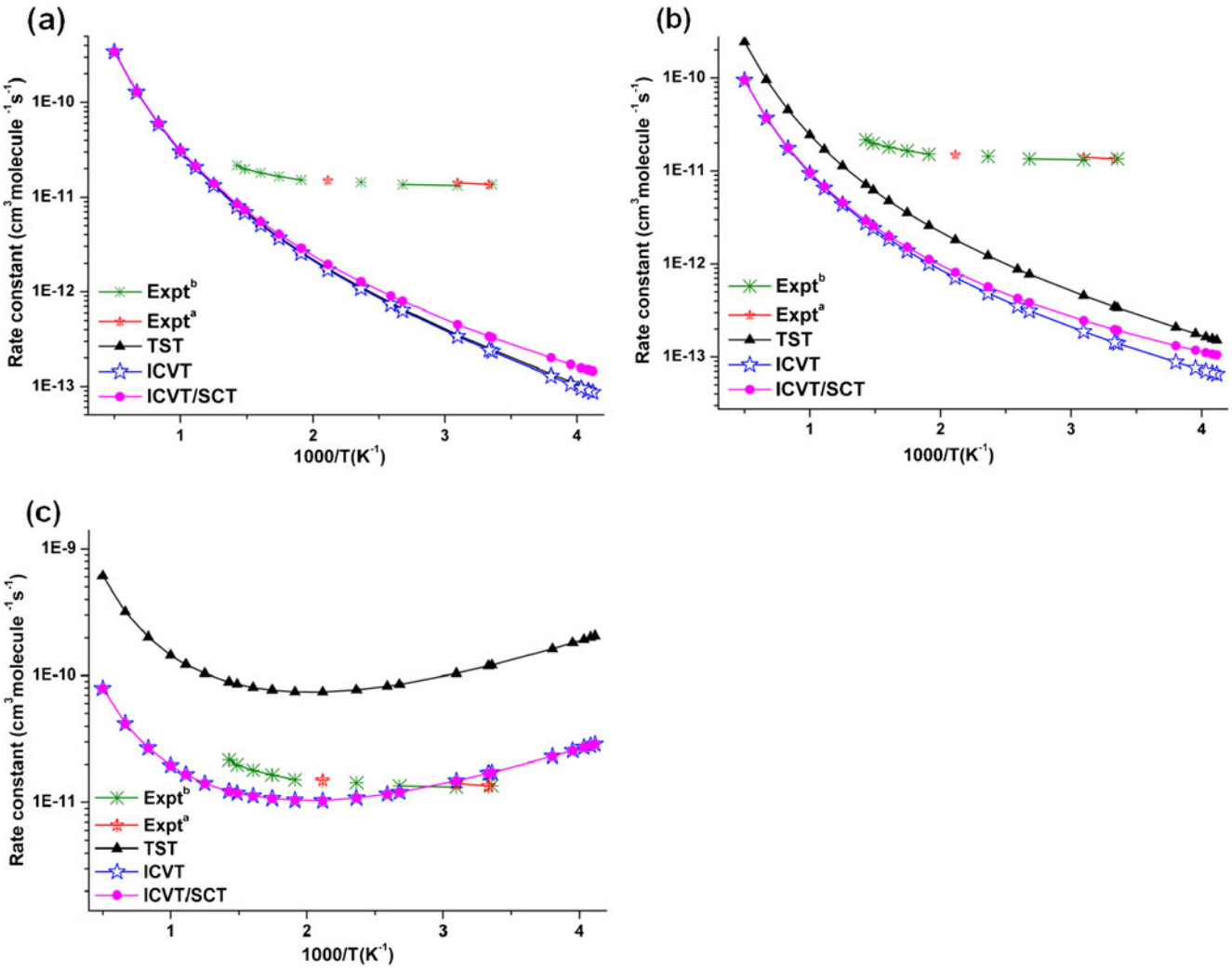

Fig. 6 Plot of the TST, ICVT, and ICVT/SCT rate constants for the **channel 1** (**a**), **channel 2** (**b**), and **channel 3** (**c**) of the title reaction at the CCSD(T)/B3//MP2/B1 level versus 1000/T between 243 and 2000 K. Expt[a], ref.[16]; Expt[b], ref.[28]

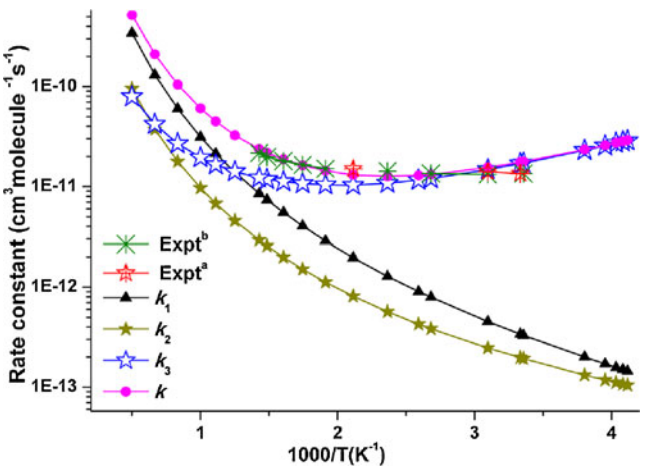

Fig. 7 Plot of the calculated individual ICVT/SCT rate constants k_1, k_2 and k_3, the overall rate constant k, and the available experimental values versus 1000/T between 243–2000 K. Expt[a], ref. [16]; Expt[b], ref. [28]

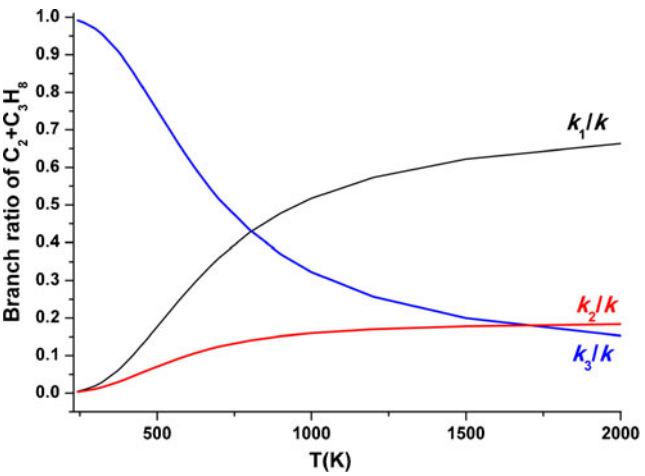

Fig. 8 Calculated branching ratios versus T between 243–2000 K

range by comparing the TST rate constants with ICVT and ICVT/SCT ones, indicating variational effect is important in rate constant calculations for channel 3. The ICVT and ICVT/SCT rate constants are in good agreement with each other, implying the small-curvature tunneling effect is negligible in the whole temperature range. Furthermore, one can find that the rate constants significantly increase as temperature decrease, indicating a negative temperature dependence occurs in this temperature range. The ICVT/SCT rate constants k_1 (channel 1), k_2 (channel 2), k_3 (channel 3) and the overall rate constant k ($k=k_1+k_2+k_3$) along with the available experimental values are plotted against 1000/T (k^{-1}) as shown in Fig. 7. From Fig. 7, we can see that the deviation between the theoretical and experimental values remains within a factor of approximately 0.8 to 1.2. In contrast to the case of CH_4 [31] and C_2H_6 [32], the temperature dependences of k shows strongly curved non–Arrhenius behavior for the $C_2+C_3H_8$ reaction. The temperature dependence of product branching ratios (k_1/k, k_2/k and k_3/k) covering the entire temperature range is demonstrated in Fig. 8. We can see that k_3 is greater than k_1 by about 198.6 to 1.4 orders of magnitude in the temperature range 243–700 K, and greater than k_2 by about 274.3 to 1.1 in the temperature range of 243–1500 K. Furthermore, the formation of $C_2H+CH_3CHCH_3$ is dominant below 700 K and the branching ratio accounts for 52–99 %, while T>700 K, $C_2H+CH_3CH_2CH_2$ products become dominant and the branching ratio accounts for 51–85 % among these channels. Consequently, the primary hydrogen atoms abstraction (channel 1 and channel 2) is expected to be dominant when T>700 K, whereas the secondary hydrogen abstraction (channel 3) is more favorable in T<700 K temperature region. The present calculated rate constants are 5.7 %–31.1 % smaller than the available experimental values [8, 16, 28]. The large discrepancy may come from the basis set size and the frequency mode in the transition state calculation. In the present work, the basis set somewhat overestimates barrier heights. This is a parameter to which the tunneling rate constant is extremely sensitive. As we know, the rate constant prediction is extremely sensitive to the calculated barrier height. Therefore, it is expected that the results should be better if single point energy refinements can be performed at the CCSD(T) level with larger basis sets. On the other hand, the prediction of one or few vibrational modes might not be accurate. It might lead to considerable errors for the calculation of V_a^G and partition function. The optimization of the transition state at higher level of theory (extremely consuming CPU time) might be better, but it is not guaranteed.

To facilitate the future experimental measurements, considering the fit in normal Arrhenius form ln$k$ versus 1/T turned out not to yield a reasonable linear relationship, we used here the conventionally adopted three (k^3) and four–parameter (k^4) rate-temperature expression as suggested by Truhlar [55] recently to fit the ICVT/SCT rate constants of the title reaction in temperature ranges from 243 to 2000 K and the expressions are given as follows (in units of cm^3 $molecule^{-1}s^{-1}$).

$$k^3(243-298\ \mathrm{K}) = 3.03\times10^{-19}(\mathrm{T})^{2.38}\exp(\frac{1290.2}{\mathrm{T}})$$

$$k^3(298-2000\ \mathrm{K}) = 3.98\times10^{-26}(\mathrm{T})^{4.77}\exp(\frac{1944.1}{\mathrm{T}})$$

$$k^4(243-298\ \mathrm{K}) = 2.57\times10^{-9}(\frac{\mathrm{T}}{300})^{-5.22}\exp\left[-\frac{1.89\times10^4(322.08+\mathrm{T})}{\mathrm{R}((322.08)^2+\mathrm{T}^2)}\right]$$

$$k^4(298-2000\ \mathrm{K}) = 1.26\times10^{-8}(\frac{\mathrm{T}}{300})^{-0.08}\exp\left[-\frac{4.18\times10^4(898.26+\mathrm{T})}{\mathrm{R}(898.26^2+\mathrm{T}^2)}\right]$$

Conclusions

In this paper, we have employed direct ab initio kinetics method to explore the reaction mechanism and the kinetics of reaction $^3C_2+C_3H_8$. Two types of hydrogen abstraction from C_3H_8 by $^3C_2$ radical have been considered. According to the IRC pathways, the electron transfer behaviors were also analyzed by quasi–restricted orbital method in detail, which shows that they take place via H–abstraction scenario conclusively.

The overall rate constants and individual rate constants (k_1, k_2 and k_3) were calculated using the TST, ICVT, and ICVT/SCT methods at the CCSD(T)/B3//MP2/B1 levels of theory over a wide temperature range 243–2000 K. From the overall rate constants prediction, variational effect and SCT correction should be taken into account in the rate constants calculations over the whole temperature region. The ICVT/SCT rate constants are in agreement with available experimental data. The predicted results show that the rate constants of these channels are temperature dependent: 1) the formation of $C_2H+CH_3CHCH_3$ is dominant below 700 K; whereas 2) when T>700 K, $C_2H+CH_3CH_2CH_2$ product channel become dominant. A negative temperature dependence of the rate constants for the reaction of $^3C_2+C_3H_8$ was observed. The three (k^3) and four–parameter (k^4) rate-temperature expressions are also provided within 243–2000 K. Our theoretical study may be useful for further insight into the reaction kinetics behavior over a wide temperature range where no experimental data is available so far.

Acknowledgments This work is supported by the National Natural Science Foundation of China (NSFC No. 21073075), Research Fund for the Doctoral Program of Higher Education of China (RFDP No. 20100061110046), the Special Funding of State Key Laboratory of Theoretical and Computational Chemistry, Jilin University and Basic Research Fund of Jilin University (No. 421010061439, 450060445067) and Graduate Innovation Fund of Jilin University (No.20121036). The authors are thankful for the reviewers' invaluable comments.

References

1. Kruse T, Roth P (1999) Int J Chem Kinet 31:11–21
2. Mckellar AR (1960) J Astron Soc Can 54:97
3. Lambert DLM (1974) Bull Astron Inst Czech 25:216
4. Chaffee FH Jr, Lutz BL, Black JH, Vanden Bout PA, Snell RL (1980) Astrophys J 236:474
5. Danks AC, Lambert DL (1983) Astrophysics 124:188
6. Huang C, Zhu Z, Wang H, Pei L, Chen Y (2005) J Phys Chem A 109:3921
7. Huang C, Li Z, Zhao D, Xin Y, Pei L, Chen C, Chen Y (2004) Chin Sci Bull 49:438
8. Huang C, Zhu Z, Xin Y, Pei L, Chen C, Chen Y (2004) J Chem Phys 120:2225
9. Donnelly VM, Pasternack L (1979) Chem Phys 39:427–432
10. Reisler H, Mangir M, Wittig C (1979) J Chem Phys 71:2109–2117
11. Reisler H, Mangir M, Wittig C (1980) Chemical Physics 47:49–58
12. Pasternack L, Baronavski AP, McDonald JR (1980) J Chem Phys 73:3508–3510
13. Ballik EA, Ramsay DA (1959) J Chem Phys 31:1
14. Mangir MS, Reisler H, Wittig C (1980) J Chem Phys 73:829–835
15. Reisler H, Mangir MS, Wittig C (1980) J Chem Phys 73:2280–2286
16. Pasternack L, Pitts WM, McDonald JR (1981) Chem Phys 57:19–28
17. Pitts WM, Pasternack L, McDonald JR (1982) Chem Phys 68:417–422
18. Skell PS, Jackman LM, Ahmed S, McKee ML, Shevlin PB (1989) J Am Chem Soc 111:4422–4429
19. Gong M, Bao Y, Urdahl RS, Jackson WM (1994) Chem Phys Lett 217:210
20. Maluendes SA, McLean AD, Herbst E (1994) Chem Phys Lett 217:571–576
21. Horner DA, Curtiss LA, Gruen DM (1995) Chem Phys Lett 233:243–248
22. Blunt VM, Lin H, Sorkhabi O, Jackson WM (1996) Chem Phys Lett 257:347–350
23. Huang C, Zhao D, Pei L, Chen C, Chen Y (2004) Chem Phys Lett 389:230–235
24. Mebel AM, Kislov VV, Kaiser RI (2006) J Phys Chem A 110:2421–2433
25. Paramo A, Canosa A, Le Picard SD, Sims IR (2006) J Phys Chem A 110:3121–3127
26. Daugey N, Caubet P, Bergeat A, Costes M, Hickson KM (2008) Phys Chem Chem Phys 10:729–737
27. Paramo A, Canosa A, Le Picard SD, Sims IR (2008) J Phys Chem A 112:9591–9600
28. Hu R, Zhang Q, Chen Y (2010) J Chem Phys 132:164312–164317
29. Canosa A, Paramo A, Le Picard SD, Sims IR (2007) Icarus 187:558
30. Pasternack L, McDonald JR (1979) Chem Phys 43:173
31. Huo RP, Huang XR, Li JL, Zhang X, Sun CC (2012) Int J Quantum Chem 112:1078–1085
32. Li N, Huo RP, Zhang X, Huang XR, Li JL, Sun CC (2011) Chem Phys Lett 503:210–214
33. Huo RP, Zhang X, Huang XR, Li JL, Sun C C (2012) Mol Phys 1–13.
34. Schlegel HB (1986) J Chem Phys 84:4530
35. Gonzalez C, Schlegel HB (1989) J Chem Phys 90:2154
36. Scuseria GE, Schaefer HF (1989) J Chem Phys 90:4
37. Pople JA, Gordon MH, Raghavachari K (1989) J Chem Phys 87:8
38. Lee TJ, Taylor PR (1989) Int J Quant Chem Symp 23:199
39. Rienstra-Kiracofe JC, Allen WD, Schaefer HF (2000) J Phys Chem A 104:9823
40. Frisch MJ, Trucks GW, Schlegel HB, Scuseria GE, Robb MA, Cheeseman JR, Montgomery JA Jr, Vreven T, Kudin KN, Burant JC, Millam JM, Iyengar SS, Tomasi J, Barone V, Mennucci B, Cossi M, Scalmani G, Rega N, Petersson GA, Nakatsuji H, Hada M, Ehara M, Toyota K, Fukuda R, Hasegawa J, Ishida M, Nakajima T, Honda Y, Kitao O, Nakai H, Klene M, Li X, Knox JE, Hratchian HP, Cross JB, Bakken V, Adamo C, Jaramillo J, Gomperts R, Stratmann RE, Yazyev O, Austin AJ, Cammi R, Pomelli C, Ochterski JW, Ayala PY, Morokuma K, Voth GA, Salvador P, Dannenberg JJ, Zakrzewski VG, Dapprich S, Daniels AD, Strain MC, Farkas O, Malick DK, Rabuck AD, Raghavachari K, Foresman JB, Ortiz JV, Cui Q, Baboul AG, Clifford S, Cioslowski J, Stefanov BB, Liu G, Liashenko A, Piskorz P, Komaromi I, Martin RL, Fox DJ, Keith T, Al-Laham MA, Peng CY, Nanayakkara A, Challacombe M, Gill PMW, Johnson B, Chen W, Wong MW, Gonzalez C, Pople JA (2004) Gaussian 03, Revision D.02. Gaussian, Inc, Wallingford, CT
41. Corchado J C, Chuang Y Y, Fast P L, HuW P, Liu Y P, Lynch G C, Nguyen K A, Jackels C F, Ramos A F, Ellingson B A, Lynch B J, Zheng J, Melissas VS, Villàa J, Rossi I, Coitino E L, P Jingzhi, Albu TV (2007) Department of Chemistry and Supercomputing Institute; University ofMinnesota: Minneapolis, MN, Version 9.7
42. Liu YP, Lynch GC, Truong TN, Lu DH, Truhlar DG, Garrett BC (1993) J Am Chem Soc 115:2408
43. Garrett BC, Truhlar DG (1979) J Chem Phys 70:1593
44. Garrett BC, Truhlar DG (1979) J Am Chem Soc 101:4534
45. Neese F (2006) J Am Chem Soc 128:10213
46. Neese F. ORCA -an ab initio, density functional and semiempirical program package, Version 2.8, Bonn University.
47. Pettersen EF, Goddard TD, Huang CC, Couch GS, Greenblatt DM, Meng EC, Ferrin TE (2004) J Comput Chem 25:1605
48. Hu WP, Rossi I, Corchado JC, Truhlar DG (1997) J Phys Chem A 101:6911
49. Gray HB (1973) Chemical Bonds. Benjamin, Menlo Park,CA
50. Hellwege KH, Hellwege AM (Eds.) (1976) Landolt-Bornstein: group II: Atomic and molecular physics vol 7: structure data of free polyatomic molecules. Springer, Berlin
51. Kuchitsu KE (1998) Structure of free polyatomic molecules - basic data. Springer, Berlin
52. Li JL, Gen CY, Huang XR, Sun CC (2006) J Chem Theory Comput 2:1551
53. Malick DKPGA, Montgomery JA (1998) J Chem Phys 108:5704
54. Huo RP, Zhang X, Huang XR, Li JL, Sun CC (2011) J Phys Chem A 115:3576–3582
55. Zheng J, Truhlar DG (2010) Phys Chem Chem Phys 12:7782